Blade Angle Effects on the Flow in a Tank Agitated by the Pitched-Blade Turbine

Yeng-Yung Tsui[1]
Professor
e-mail: yytsui@mail.nctu.edu.tw

Jian-Ren Chou
Graduate Student

Yu-Chang Hu
Graduate Student

Department of Mechanical Engineering,
National Chiao Tung University,
Hsinchu 300, Taiwan R. O. C.

This paper presents a study of the influence of the blade angle on the flow in a tank stirred by the pitched-blade turbine. The flow induced by the pitched-blade turbine is usually described as an axial type with a principal ring vortex dominating the flow structure. However, it is known that as the blade becomes vertical, i.e., as the pitch angle of the blade becomes 90 deg*, the flow is of the radial type, with two main ring vortices occupying the tank. Thus, a transition of flow type must take place when the blade angle is varied. This motivates the current study. A computational method was developed, which incorporates the unstructured grid technique to deal with the complex geometry in the tank. Multiframe of reference was employed to handle the rotation of the impeller. The results show that the transition from the axial type to the redial type is not progressive, but occurs all of a sudden at a particular angle, depending on the configuration. This critical angle decreases as the off-bottom clearance and the impeller size are increased. Its influences on the flow angle of the discharge stream, the power requirement, the induced flow rate through the impeller, and the pumping efficiency are discussed. The mechanism to cause the sudden change of flow type is addressed through observing the flow on the surface of the turbine blade.* [DOI: 10.1115/1.2201636]

1 Introduction

Flow agitation is an important process in the chemical and biotechnical industries. It is usually used to blend different liquids, erase concentration or temperature gradients, perform chemical reactions or biotechnical conversions, and for suspension of solid particles or dispersion of gases in liquids. To agitate the fluid a rotating impeller is introduced into the tank. For fluid mixing the contact surface between the fluids is distorted by the agitated flow, leading to elongation of the interface. As a result of the elongated interface, the mixing rate is accelerated since the gradients in the contact surface are smoothed out by the molecular diffusion. This process can be further enhanced in the turbulent field because the contact surface is largely wrinkled by turbulent fluctuations.

The most popular agitator adopted in the industry is either the disc-type flat-blade turbine, referred to as the Rushton turbine, or the pitched-blade turbine. For the former a number of flat blades are vertically installed on the periphery of a disc. The centrifugal force caused by the rotating impeller generates a radial jet stream. After impinging of the jet on the wall of the tank, two ring vortices are formed: one occupies the upper volume of the tank and the other the lower part. This kind of flow is termed radial style [1]. There is no disc installed in the pitched-blade turbine. The blades are inclined to the horizontal plane to form a blade angle. Different from the Rushton turbine, for which the discharge stream emerges from the periphery of the impeller, the flow of the pitched-blade turbine is discharged from the lower side of the blade passages. Therefore, it is a large ring vortex dominating the flow pattern in the stirred tank. This is called axial style [1]. In addition to the ring vortices, trailing vortices were observed in the low pressure regions behind the blades in both types of agitators [2–5]. The trailing vortex possesses the characteristic of high shear stress and has a beneficial effect on generation of turbulence. This is helpful to flow mixing and particle dispersion.

In this study we are concerned with the pitched-blade turbine. The geometry of the impeller has significant effects on its performance. Ranade and Joshi [6] used the laser Doppler anemometer to examine the flow characteristics in certain ranges of blade angles (30 deg–60 deg), blade widths (0.2 D–0.4 D), and impeller diameters (0.25 T–0.5 T). The pumping capacities and hydraulic efficiencies have also been reported. It was indicated that the hydraulic efficiency increases with the blade angle and the impeller diameter within the range studied. Besides the dominant vortex mentioned above, there may exist a smaller vortex, also induced by the discharge stream, located at the center region below the impeller. The influence of the impeller geometry on these vortex flows was conducted by Mao et al. [7]. The pumping numbers of the primary and secondary vortices were reported. The off-bottom clearance has great impact on the strength of the secondary vortex [7–9]. At low clearances, the secondary vortex is restricted in the center region. As the clearance becomes large, the discharge stream is directed toward the horizontal direction and the secondary vortex expands in size.

It is interesting to notice from the studies by Nouri and Whitelaw [10] and Hockey and Nouri [11] that a change of the flow pattern can take place by reducing the rotating speed, i.e., the Reynolds number. The measurements of axial velocity by Nouri and Whitelaw imply a rapid shift from an axial flow to a radial flow at a Reynolds number of around 650 while the sharp drop of power consumption measured by Hockey and Nouri indicates a transition of flow pattern at a Reynolds number of 1200. The difference in the critical Reynolds number is ascribed to different impeller sizes used.

In view of the above studies the configuration of the agitator setup has a decisive influence on the flow structure and its performance. It was seen that although, in general, the axial type of flow will be formed, it may be transformed into the radial type by choosing different off-bottom clearances or rotating speeds. Later in this study similar phenomena will be observed by varying the blade angle.

Computational fluid dynamics (CFD) provides an alternative tool for fluid flow analysis. The flow in the stirred tank is inherently periodic and unsteady. Fully time-dependent computations require excessive computer resources. The steady-state computations by Wechsler et al. [12] showed an excellent agreement with

[1]Corresponding author.

Contributed by the Fluids Engineering Division of ASME for publication in the JOURNAL OF FLUIDS ENGINEERING. Manuscript received May 1, 2005; final manuscript received January 24, 2006. Assoc. Editor: Akira Goto.

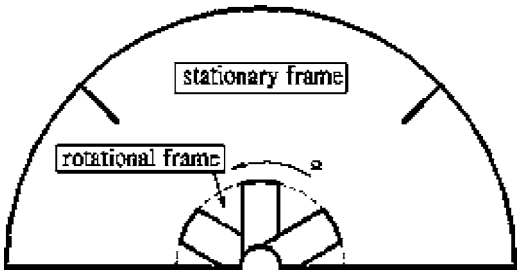

Fig. 1 Multiframe of reference

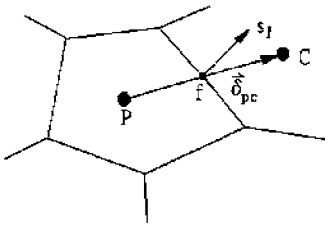

Fig. 2 Illustration of a control volume

fully unsteady computations, but at a fraction of expense. Thus, for engineering analysis it is sufficient to assume a quasisteady state. In the steady-state model the impeller is fixed at a particular position relative to the wall of the tank and the grids are stationary without moving. However, the flow in the tank needs to be induced in calculations with some methods. In the early stage measured profiles of mean velocity and turbulence were prescribed around the impeller as boundary conditions [13–17]. In this way, extensive experimental work is required. Thus, the usefulness of this approach is severely restricted. Xu and McGrath [18] treated the impeller blades as airfoils. The lift and drag forces produced on the airfoils are implemented as a momentum source to drive the flow. Ranade and Dommeti [19] described the interaction between the fluid and the blades by applying appropriate mass and momentum sources at the blade surface. Recently, a popular method adopted is to mount the blade-swept volume on a rotating frame of reference and the rest part of the tank on the stationary frame [12,20]. The body forces generated by the rotating frame will trigger the fluid flow.

In the present study the multireference frame is employed to model the three-dimensional turbulent flow in a tank stirred by the pitched blade turbine. To cope with the complex geometry prevailed in the tank, unstructured grids are used. The turbulence needs to be characterized by turbulence models. A number of turbulence models, including Reynolds stress model [15,17], algebraic stress model [16], and variant k-ε and k-ω models [21,22] have been tested. In general, all these models obtained an overall qualitative agreement with measurements, but poor predictions in some parts of the tank, especially in the discharge region. There is no particular model much superior to the others. Hence, the most popular k-ε model is adopted in the present computations. Under different settings of configuration we will examine the transition of the flow structure by varying the blade angle. The effects on the flow and the performance will be shown.

2 Mathematical Method

As shown in Fig. 1, the tank is divided into two parts. The blade-swept region rotates with the impeller while the other region is fixed without moving. Define the grid velocity as

$$\vec{U}_g = \vec{\Omega} \times \vec{r} \text{ in the blade-swept region} \tag{1a}$$

$$\vec{U}_g = 0 \text{ in the stationary region} \tag{1b}$$

where $\vec{\Omega}$ is the angular speed of the impeller and $\vec{r}$ the position vector of the considered nodal point. The continuity equation and the transport equations in the Cartesian coordinates can then be cast into the following form:

$$\frac{\partial}{\partial x_j}[\rho(U_j - U_{gj})] = 0 \tag{2}$$

$$\frac{\partial}{\partial x_j}[\rho(U_j - U_{gj})\phi] = \frac{\partial}{\partial x_j}\left(\Gamma_\phi \frac{\partial \phi}{\partial x_j}\right) + S_\phi \tag{3}$$

where ϕ represents $U_j - U_{gj}$, k, and ε, ρ is the fluid density, and Γ_ϕ the diffusion coefficient. $U_j - U_{gj}$ denotes the flow velocity with respect to the grid. In the momentum equation the rotation-induced body forces, including centrifugal force and Corriolis force, must be accounted for as sources.

$$S'_{U_j} = -\rho\varepsilon_{mnj}\Omega_m(\varepsilon_{pqn}\Omega_p x_q) + 2\rho\varepsilon_{mnj}\Omega_m(U_n - U_{gn}) \tag{4}$$

Here, ε_{ijk} is the alternating unit tensor. It is noted that in the stationary region S'_{U_j} must be set to zero. The turbulence is characterized by the standard k-ε model of Launder and Spalding [23]. The wall function is used to bridge the near wall region to avoid excessive grid nodes there.

To deal with the irregular geometry in the tank one method is to use block-structured grids, as done by Harvey et al. [20] and Wechsler et al. [12]. In this way the blocks are globally unstructured, but the grids are locally structured. Transformation of the coordinate system is necessary, rendering the governing equations much more complicated. In addition, a solution must be iterated among the blocks. Special care must be taken at each interface between neighboring blocks to ensure coupling. An alternative, which can circumvent the above inconveniences, is the use of unstructured grids. To construct difference equations the differential equations are integrated over a control volume. By applying the divergence theorem of Gauss the volume integrals for the convection and diffusion terms are then transformed into surface integrals. The convection and diffusion fluxes through the surface of the control volume can be expressed as

$$F^c = \sum_f [\rho(\vec{V} - \vec{V}_g) \cdot \vec{s}]_f \phi_f \tag{5a}$$

$$F^d = \sum_f (\Gamma \nabla \phi \cdot \vec{s})_f \tag{5b}$$

where the subscripts f denote the faces of the control volume, $\vec{s}_f$ is the surface vector of the considered face (see Fig. 2), and the summation is taken over all the faces. In the convection flux the face value is approximated by

$$\phi_f = \phi^{\mathrm{UD}} + \gamma(\nabla\phi)^{\mathrm{UD}} \cdot \vec{\delta} \tag{6}$$

Here the superscripts UD denote the value evaluated at the adjacent node in the upwind direction of the face, $\vec{\delta}$ is the distance vector directed from the upwind node to the centroid of the face. In the equation, γ is a blending factor between 0 and 1. For a value of 0 it represents an upwind difference scheme, and for a value of 1 a second-order scheme. In the following computations, 0.9 is assigned to γ.

The diffusion flux is estimated by the following approximation:

$$F^d = \frac{\Gamma_f s_f^2}{\vec{\delta}_{PC} \cdot \vec{s}_f}(\phi_C - \phi_P) + \Gamma_f \overline{\nabla\phi}_f \cdot \left(\vec{s}_f - \frac{s_f^2}{\vec{\delta}_{PC} \cdot \vec{s}_f}\vec{\delta}_{PC}\right) \tag{7}$$

where, see Fig. 2, the superscripts P and C denote the principal and the neighboring nodes sharing a common face, and $\vec{\delta}_{pc}$ is a

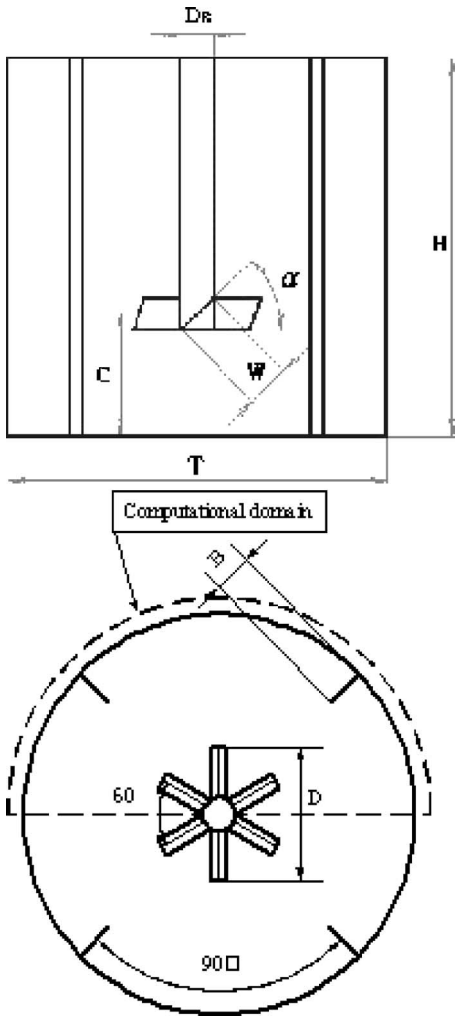

Fig. 3 A sketch of a stirred tank

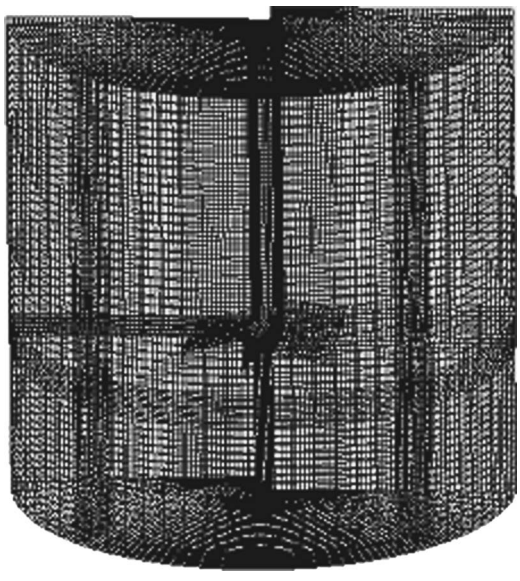

Fig. 4 A typical computational grid

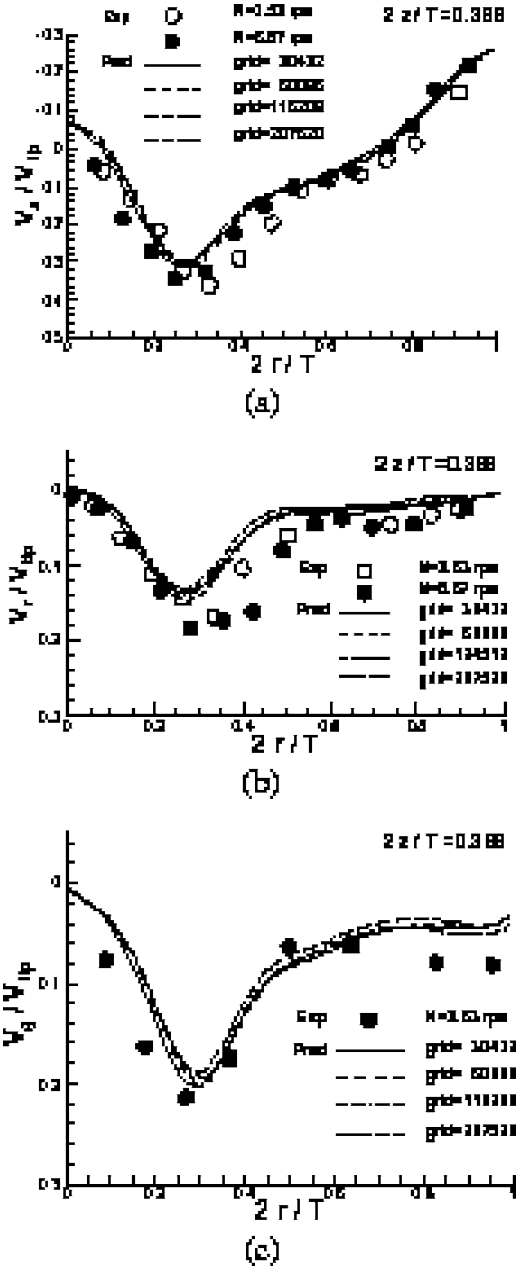

Fig. 5 Comparison of predictions with measurements

vector connecting these two nodes. The face gradient $\overline{\nabla\phi}_f$ is obtained via interpolation from the values at the two nodes P and C.

It needs to be noted that the computational molecule for the nodes next to the interface between the two reference frames comprises nodes in the other frame. The velocity at these neighboring nodal points must be transformed onto the same frame as the one for the principal node P to evaluate the momentum flux transported through the interface.

The coupling between the momentum and continuity equations are treated according to the SIMPLE (Semi-Implicit Method for Pressure-Linked Equations) algorithm. The velocity and pressure are collocated on the centroid of each control volume. To avoid decoupling between velocity and pressure fields the momentum interpolation technique is applied. More details about this method are referred to in the study by Tsui and Pan [24].

The baffles and the impeller are arranged in a symmetrical manner, as seen in Fig. 3. Due to the symmetrical arrangement the flow becomes periodic. Therefore, only half the tank is considered in calculations and periodic conditions are imposed on the symmetrical boundary planes. The fluxes out of the 0 deg radial plane must be carried into the 180 deg plane, and vice versa. To ensure a correct transfer of fluxes auxiliary control volumes along the

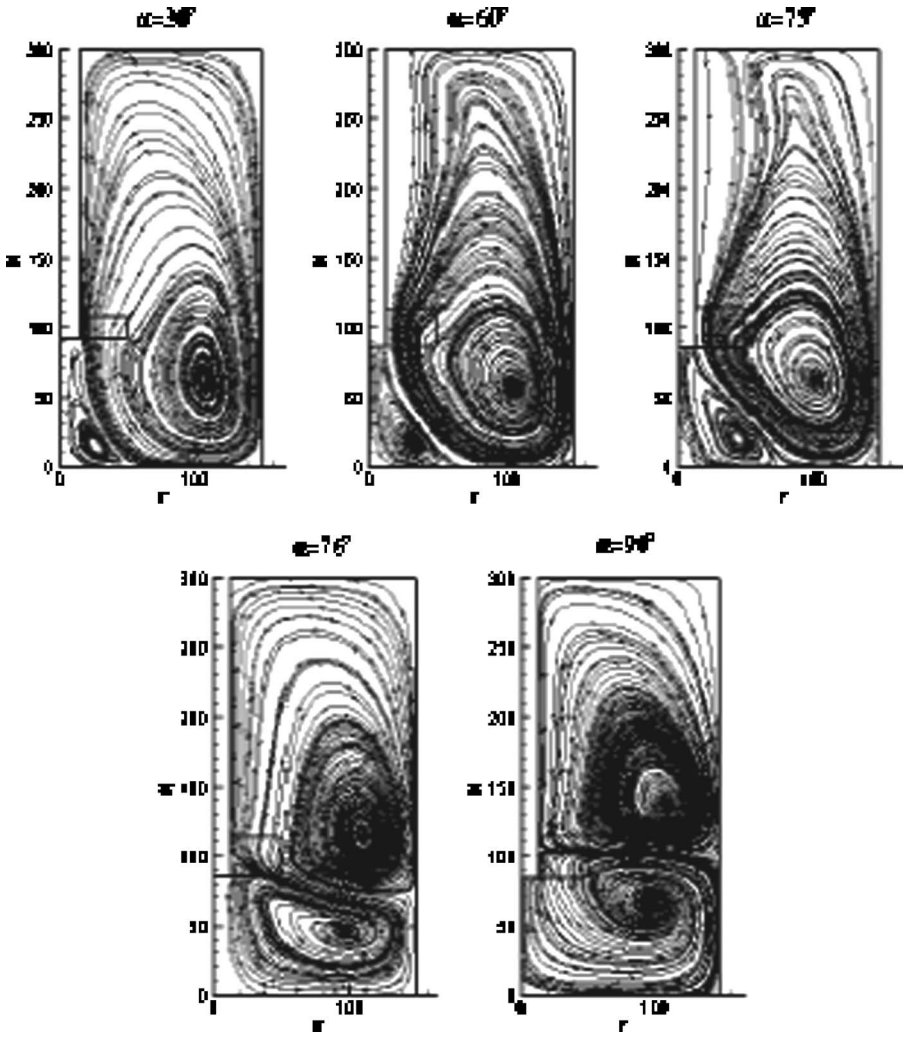

Fig. 6 Flow streamlines for $D=T/3$, $C=T/3$

symmetrical planes are added. The boundary data in the auxiliary control volumes is updated after each outer iteration of the SIMPLE algorithm.

3 Results and Discussion

A sketch of a typical stirred tank is shown in Fig. 3. The diameter of the tank is denoted as T, and the height of the tank as H. There are four equally-spaced baffles fitted on the surrounding wall with a width B. The clearance of the impeller is C, which is measured from the center line of the blade to the bottom of the tank. The impeller holds six blades and has a diameter D. The blades have a pitch angle α and a width W. To generate unstructured grids the computational domain is first divided into 40 blocks. In each block a simple method, such as an algebraic method, is used to create a suitable grid. After the grids for all the blocks are constructed, the grid nodes are readdressed. An example of the resulted grid is presented in Fig. 4.

To validate the current mathematical model, computations have been performed to compare with the measurements of Ranade and Joshi [6]. The specifications of the stirred tank configuration studied by them are: $T=H=300$ mm, $D=C=100$ mm, $W=B=30$ mm, and $\alpha=45$ deg. To examine the grid sensitivity of the solution four different levels of grids were tested, including node numbers of 30,432, 60,096, 116,208, and 207,520. Figure 5 presents the predicted velocity components V_z, V_r, V_θ in the axial, radial, and circumferential directions at an axial station $2z/T=0.366$ below the center of the impeller blade. In the figure V_{tip} represents the blade tip velocity. The rotational speed is set at $N=3.53$ rps, i.e., at a Reynolds number ($=\rho ND^2/\mu$) of 3.53×10^4. Another set of measurements for $N=6.67$ rps is also included for comparison. It can be seen that the velocities are accelerated quickly to reach a position roughly corresponding to the tip of the blade, followed by a gradual decrease. The negative axial velocity in the region near the side wall of the tank implies the existence of a circulation loop, i.e., an axial vortex there. The predictions capture these characteristics quite well, though, in comparison with measurements, some degree of discrepancy exists. More comparison in terms of pumping number and power number will be given later. Not much difference was observed for different grids used. In the following, the grid with about 120,000 nodes is adopted. It needs to be emphasized here that the disagreement between the predictions and the measurements is partly attributed to the imperfection of the eddy viscosity model which cannot cope with such a complex vortex and swirling flow. Another factor affecting the prediction accuracy is the assumption of steady state. In a real situation the impeller blades keep changing their position relative to the baffles, but not in the numerical simulation. It is noted that the experiments conducted by Ranade and Joshi were obtained over 360 deg of impeller revolution, i.e., the time averaging was undertaken. The angle-resolved measurements for a pitched-blade turbine by Hockey and Nouri [11] revealed a variation of the mean velocity and the turbulence fluctuation with the revolution

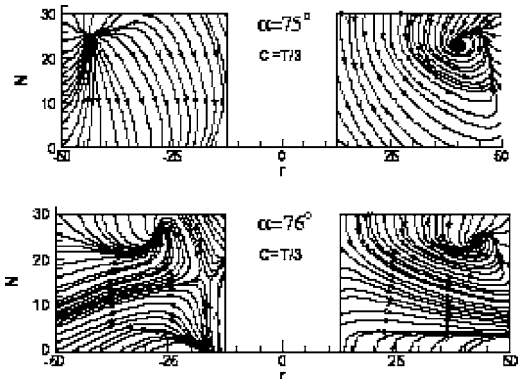

Fig. 7 Limiting streamlines on the surface of the blade for α =75 deg and 76 deg. The sketches on the left are referred to the front surface and those on the right to the back surface.

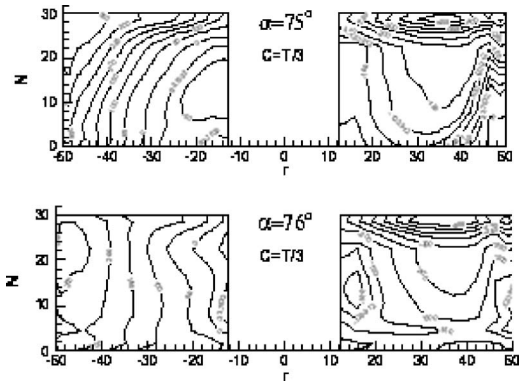

Fig. 8 Pressure contours on the surface of the blade for α =75 deg and 76 deg. The sketches on the left are referred to the front surface and those on the right to the back surface.

angle. It was shown by them that the blade-to-blade differences in the mean velocity and the root-mean square (rms) fluctuation are within 5% in the 1.08 deg angle-resolved measurements. The time averaging can lead to an overestimate of the rms fluctuation by up to twofold. The blade-to-blade variation of the mean velocity surely contributes to the rms fluctuation in the time-averaging. However, the cause of the overestimate of the turbulent fluctuation is mainly due to the periodic variation in the mean velocity.

The blade angle α is varied first while the other parameters remain the same as above. It was recognized from the experiments of Dong et al. [25] that the pitched blade turbine behaves like the Rushton turbine when the blades are in the vertical position (α =90 deg). This behavior is confirmed in Fig. 6. The flow field shown in the figure is in the midplane between two blades. It can be seen, according to this figure, that in the range α =30 deg–75 deg the flow is of the axial type, with a large circulation loop occupying most part of the tank and a much weaker one restricted in the center region below the impeller. The size of the smaller circulation loop gradually increases with the blade angle. A dramatic enlargement occurs when the blade angle is increased to 76 deg. The jet stream discharged from the impeller impinges on the side wall, instead of the bottom wall as observed in the lower blade angles. The minor circulation loop now almost overwhelms the whole volume beneath the impeller and the flow field changes from the axial type to the radial type. By further increasing the blade angle the jet stream adjusts its direction slightly until fully radial direction is reached at α=90 deg.

To gain insight into the detailed flow near the blades, the limiting streamlines, which are streamlines passing very close to the blade surface, are shown in Fig. 7 for the cases of α=75 deg and 76 deg with $C=D=T/3$. In the figure the cross sections show the two surfaces of the turbine blade. The sketches on the left are referred to the front surface of the blade and those on the right to the back side. On the front there is a repelling spiral-focal point at the upper corner near the blade tip for the subcritical angle of 75 deg. This nodal point behaves like a source, or a stagnation point, where fluid flows toward the surface and sprays over the front surface, mainly in the direction down to the lower edge. When the critical angle of 76 deg is reached, the source is shifted toward the base side. In the meanwhile, fluid is drawn from the lower edge close to the base. As a result, a saddle point is formed at the midheight position near the base. Fluid is then forced to flow radially from the saddle point toward the outer edge. At the back side, it is evident that there exists an attracting spiral-focal point which plays the role of flow sink. It draws fluid from the top side and the upper tip and transports the fluid away from the back surface. This sink simply represents the center of the trailing vortex mentioned in the Introduction. The trailing vortex is located at the upper corner near the tip, which is similar to the results reported by Schafer et al. [4] and Wechsler et al. [12]. It is interesting to note that, especially for α=75 deg, some streamlines close to the tip merge into one streamline before they end at the sink point. This behavior of merging streamlines from both sides of the streamline implies that this line segment is a line of separation, i.e., flow starts to separate here. The line of separation is not so obvious for α=76 deg.

Pressure distribution on the blade is illustrated in Fig. 8. Generally speaking, adverse pressure gradient prevails in the radial direction on the front surface due to the tendency for it to balance the centrifugal force prevailing outside the boundary layer. For α=75 deg the highest pressure is situated at the upper corner near the tip, where the stagnation point is located. For this case the pressure gradient, as well as the shear force, drives the flow from

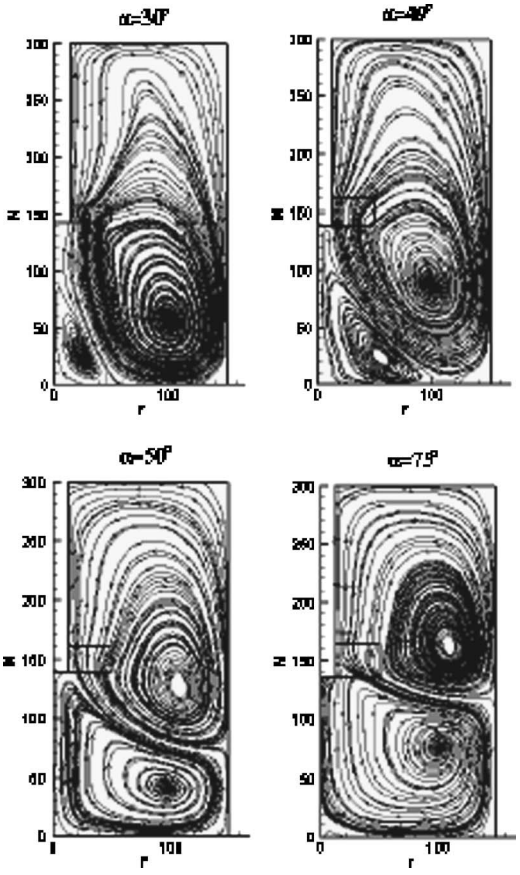

Fig. 9 Flow streamlines for $D=T/3$, $C=T/2$

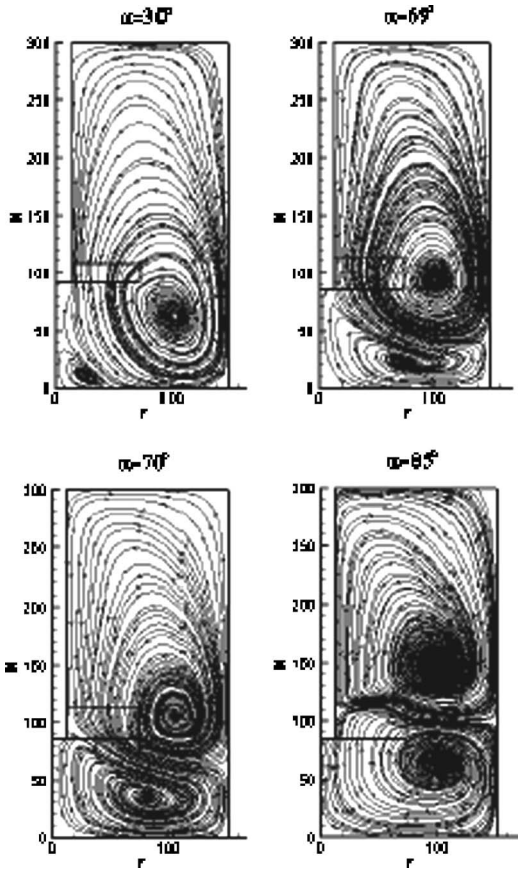

Fig. 10 Flow streamlines for $D=T/2$, $C=T/3$

the region in the upper edge to the lower edge, as seen in the previous figure. As for $\alpha=76$ deg it is mainly the shear force alone to control the fluid to flow radially outward. On the back surface the pressure is lower in comparison to the front surface, which is expected. The lowest pressure is always found at the upper edge because this is the leading edge of the blade airfoil.

In view of the above results, it can be concluded that the change of pitch angle will trigger flow instability at a specific angle. For blade angles greater than this angle, it is the centrifugal force prevailing in the blade passage to drive fluid to flow mainly in the radial direction. As the blade angle is reduced, a strong stagnation flow occurs in the upper region on the front surface, close to the blade tip. This results in a pressure gradient in the axial direction, which forces fluid to flow from the upper region to the lower region. Thus, the flow pattern is changed from the radial type to the axial type.

As mentioned in the literature review, the off-bottom clearance has a great effect on the flow. It can be seen from Fig. 9 that the transition of flow type takes place at an earlier angle of 50 deg by increasing the clearance C from $T/3$ to $T/2$. It is ready to find that for a fixed blade angle between 50 deg and 75 deg the change of the impeller clearance can result in a different flow pattern.

In order to investigate the effect of the blade length the diameter of the impeller D is increased from $T/3$ to $T/2$. As seen in Fig. 10, the critical blade angle is slightly reduced from 76 deg to 70 deg. The difference in the circulating flow structure between $\alpha=69$ deg and 70 deg is not as obvious as that for the smaller impeller case. For the smaller impeller the minor circulation loop is always limited in the center region and the flow remains to be of the axial type at all subcritical angles whereas for the larger one the discharge stream has impinged on the surrounding wall and the flow field has become a mixed type of axial/radial flow before the critical angle is reached

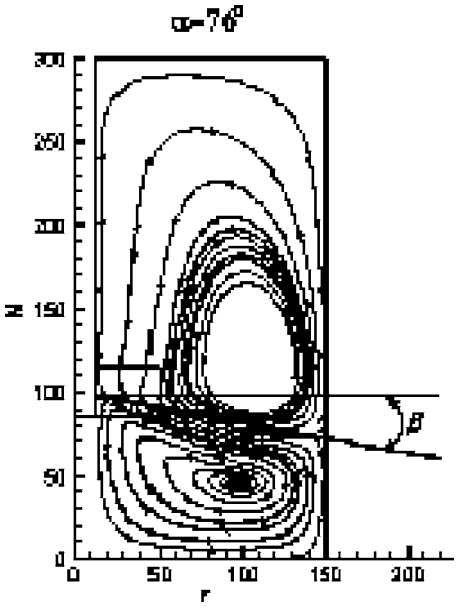

Fig. 11 Define flow angle of the discharge stream

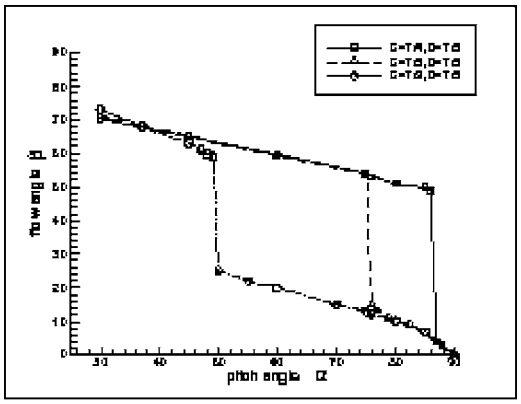

(a)

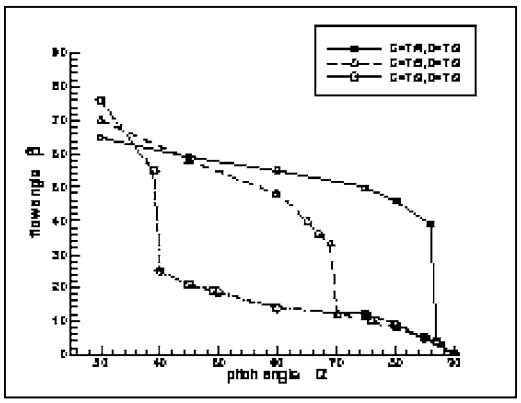

(b)

Fig. 12 Variation of the flow angle against the pitch angle of the blade for (*a*) $D=T/3$, and (*b*) $D=T/2$

An angle β, characterizing the flow orientation of the discharge stream, is defined as the inclination of the line connecting the two points separating the two circulation loops on the rotating shaft and on the wall, as illustrated in Fig. 11. The variation of this flow angle with respect to the blade angle is presented in Fig. 12. There exists a sharp drop in the flow angle at each critical blade angle. It

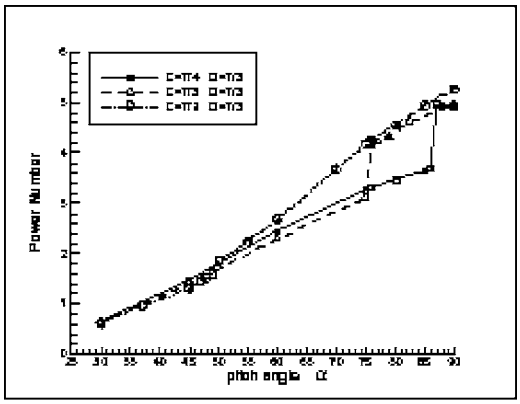

(a)

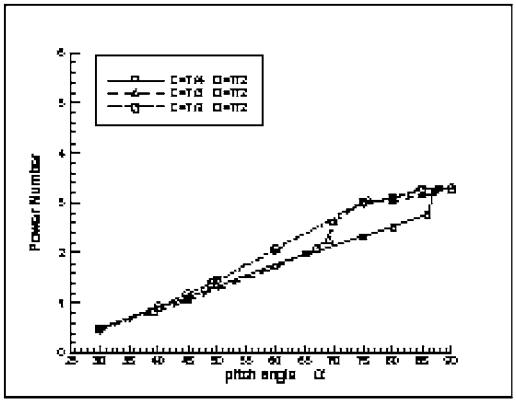

(b)

Fig. 13 Variation of the power number against the pitch angle of the blade for (*a*) *D*=*T*/3, and (*b*) *D*=*T*/2

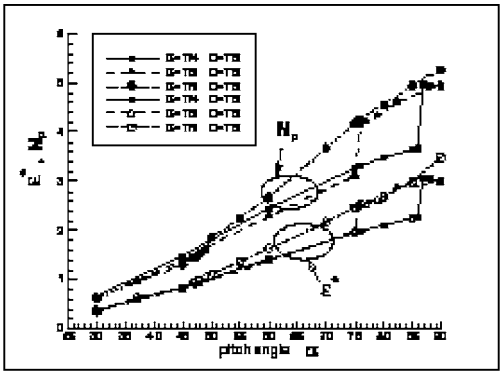

(a)

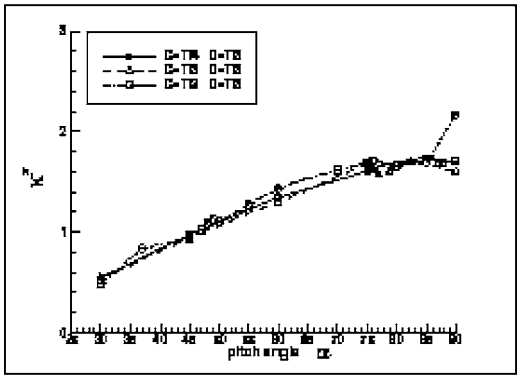

(b)

Fig. 14 Variation of (*a*) k^* and (*b*) ε^* against the pitch angle of the blade for *D*=*T*/3

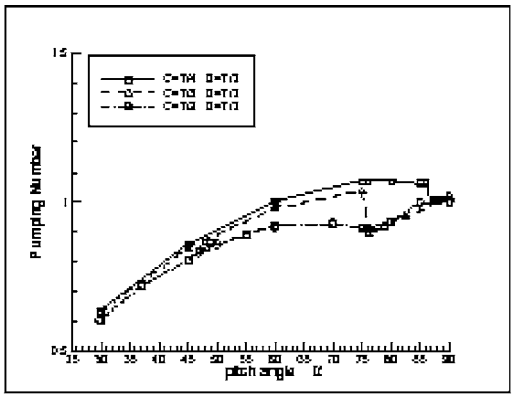

(a)

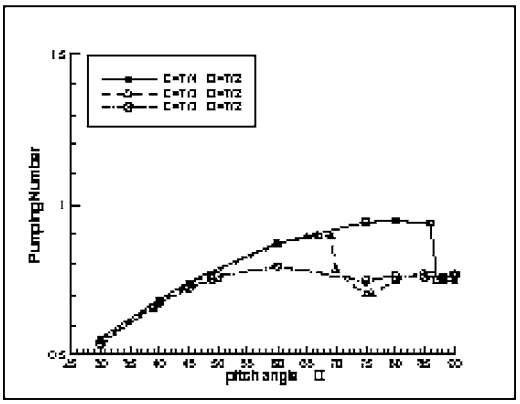

(b)

Fig. 15 Variation of the pumping number against the pitch angle of the blade for (*a*) *D*=*T*/3, and (*b*) *D*=*T*/2

is interesting to notice that for the smaller impeller case the flow angles almost fall on the same curves, being nearly linear, before and after the transition takes place. For the larger impeller case the flow angle declines first before the sharp drop occurs. The decline rate is higher as the clearance is increased. But the flow angles are on the same curve after the flow pattern changes.

The change of flow field will seriously affect the power consumption and the performance of the agitator. Power number N_p is defined by

$$N_p = \frac{2\pi N\tau}{\rho N^3 D^5} \tag{8}$$

where N represents the impeller rotational speed in rps, and τ the required torque of the impeller. The torque is calculated as the sum of the moments generated by both the pressure force exerted on the blades and the shear force exerted on the blades and the rotating shaft. The part generated by the shear force is much smaller, in general, less than 1% of the total torque. As seen in Fig. 13, the power required to drive the impeller increases with the pitch angle of the blade. There exists a jump at each critical angle. The extent of the jump decreases as the clearance and the impeller diameter are enlarged. For the case with $C=T/2$ and $D=T/2$ the jump at $\alpha=40$ deg is nearly invisible. Similar to the flow angle, the data of power number also falls on similar curves before and after the flow pattern changes.

Figure 14 shows the dependence of the total turbulent energy and its dissipation rate generated in the tank on the blade angle for $D=T/3$. Both are nondimensionalized as

$$k^* = \frac{\int_V \rho k \bullet dv}{\rho N^2 D^5} \tag{9}$$

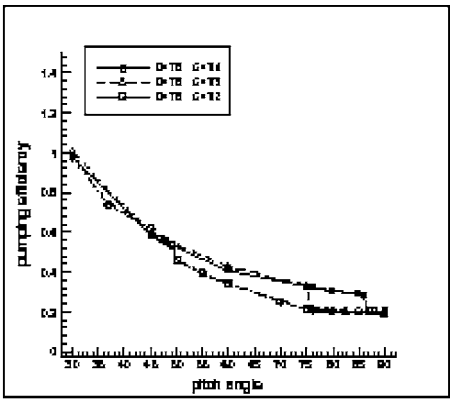

(a)

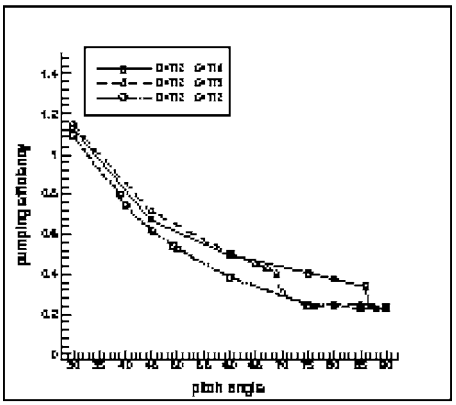

(b)

Fig. 16 Variation of the pumping efficiency against the pitch angle of the blade for (*a*) *D*=*T*/3, and (*b*) *D*=*T*/2

$$\varepsilon^* = \frac{\int_V \rho\varepsilon \bullet dv}{\rho N^3 D^5} \tag{10}$$

where the integration is taken over the entire volume of the tank. For comparison the power number shown in Fig. 13(*a*) is also included in Fig. 14(*a*). It indicates that the turbulence dissipation rate behaves in a similar manner as the power consumption, which is expected because the energy transferred from the impeller to cause the fluid flow will be cascaded into turbulence and dissipated into heat in the end. However, the total dissipation rate is much lower than the power required. Part of the reason for causing the difference is due to the inadequacy of the turbulence model. The turbulent energy produced increases with the pitch angle. However, there exists a drop at the critical angles. The drop is not as obvious as the jump in the power.

In a mixing system the circulating flow is responsible for the function of the agitation because the mixing time depends on the circulation time. This flow is originated from the stream discharged from the impeller. Therefore, the strength of the circulating flow can be characterized by the induced flow rate through the impeller. A pumping number is defined as

Table 1 A summary of critical pitch angles

	C=*T*/4 (deg)	*C*=*T*/3 (deg)	*C*=*T*/2 (deg)
D=T/3	87	76	50
D=T/2	87	70	40

$$N_Q = \frac{Q}{\rho N D^3} \tag{11}$$

where Q is the net mass flow rate through all the blade passages of the impeller. The predicted pumping numbers for the cases with $C=D=T/3$ at $\alpha=30$, 45, and 60 deg are 0.63, 0.84, and 0.98, respectively, which compares reasonably well with the experimental data of 0.6, 0.93, and 1.1 given by Ranade and Joshi [6]. Hockey and Nouri [11] reported a pumping number of 0.88 for the blade angle of 60 deg, which seems a little on the low side in comparison to the predictions and measurements by Ranade and Joshi. However, the power number of 2.2 measured by Hockey and Nouri is in very good agreement with the present value of 2.3. By increasing the impeller diameter to $D=T/2$, the predicted pumping number of 0.74 for $\alpha=45$ deg is close to the data of 0.8 obtained by Ranade and Joshi.

Figure 15 reveals that the pumping number increases with the pitch angle, but tends to level off for high angles. At the angle where the flow is transformed into the radial type the mass flux declines sharply. This phenomenon of sharp declination is more prominent in the cases with larger impellers and lower clearances.

The pumping efficiency, defined by

$$\eta = \frac{N_Q}{N_P} \tag{12}$$

is a measure of effectiveness of the impeller to generate pumping flow per unit of power input. Figure 16 shows that the pumping efficiency decreases with the blade angle and levels off when approaching 90 deg. It is especially true for the smaller impeller that all the data falls on the same curves before and after the pattern change take places. The large impeller is more efficient in circulating flow per power input because the efficiency ranges from 0.23 to 1.15 while that for the smaller impeller is in the range of 0.2–1.

The critical pitch angles are summarized in Table 1. It can be found that with the smallest clearance of $C=T/4$ the axial flow type prevails unless the blades are close to the vertical position. The critical angle is very sensitive to the clearance. The increase of clearance will cause significant decrease in this angle. The increase in the impeller size can also result in a decrease of the critical angle; with a larger impeller the transition will occur at a lower blade angle.

4 Conclusions

A computational methodology has been developed to examine the flow field in a tank agitated by a pitched-blade impeller. The flow was assumed to be in a quasisteady state. The tank was divided into two parts. The blade-swept region was situated on a rotational frame of reference and the rest on a stationary frame. Discretization was based on the unstructured mesh manner to deal with the complex geometry encountered in the tank. The effect of the pitch angle of the blade was carefully studied. A summary of the main findings is drawn in the following.

1. At low blade angles the circulating flow in the tank, generally, is of the axial type with a minor recirculation loop restricted in the center region below the impeller. The size of this small circulating flow gradually increases with the blade angle until a critical angle is reached. At this critical angle the flow is transformed into the radial type all of a sudden. With further increase of the angle to 90 deg, the pitched-blade turbine behaves like a Rushton turbine.
2. For blade angles greater than the critical angle, it is the centrifugal force which dominates in the blade passage and forces fluid to flow radially. As the pitch angle is reduced to lower than the critical angle, a strong stagnation flow is formed in the upper region on the front sur-

face of the blade, driving the fluid to flow axially downward. It is this mechanism to cause the sudden change of flow type.

3. The clearance of the impeller to the tank bottom has a significant influence on the critical angle. This critical angle decreases as the clearance increases. The enlargement of the impeller diameter may also reduce the critical angle.
4. The flow angle of the discharge stream can be regarded as a measure of the size of the smaller circulating flow. The smaller the flow angle, the larger the secondary circulation. In general, the discharge flow angle gradually decreases when the blade angle increases. However, at the critical angle a sharp drop appears, indicating a change of flow type. The extent of the sudden reduction in the flow angle is less significant for lower clearances and larger impellers.
5. The power consumption and the induced mass flow through the impeller increases with the blade angle. But the pumping efficiency decreases as the blade angle increases. The pumped flow rate and the pumping efficiency level off at large blade angles. The transition to the radial type leads to a jump in power requirement and a sharp decline in the pumped flow rate and its efficiency.

Acknowledgment

This work was supported by National Science Council of Taiwan, R.O.C., under Contract No. NSC-93-2212-E-009-012 and No. NSC-94-2212-E-009-024.

Nomenclature

B = baffle width
C = off-bottom clearance
D = impeller diameter
D_s = shaft diameter
F^c = convection flux
F^d = diffusion flux
H = tank height
k = turbulent kinetic energy
k^* = dimensionless total turbulent kinetic energy
N = rotational speed
N_P = power number
N_Q = pumping number
Q = net mass flux through all blade passages
s_f = surface vector
S_ϕ = source term of transport equation for ϕ
T = tank diameter
$\vec{U}_g, U_{gj}$ = grid velocity vector
U_j = flow velocity vector
V_r, V_θ, V_z = velocities in radial, circumferential, and axial directions
V_{tip} = blade tip velocity
W = blade width
x_j = Cartesian coordinates of the considered point
z = vertical distance

Greek Symbols

α = pitch angle
δ_{PC} = distance vector directed from P to C
ε = turbulent dissipation rate
ε^* = dimensionless total turbulent dissipation rate
ε_{ijk} = alternating unit tensor
ϕ = a flow property
γ = blending factor
Γ_ϕ = diffusion coefficient for ϕ
η = pumping efficiency
τ = torque
$\vec{\Omega}, \Omega_m$ = angular speed

Subscripts

f = face value
ϕ = for the flow property ϕ

References

[1] Tatterson, G. B., 1991, *Fluid Mixing and Gas Dispersion in Agitated Tanks*, McGraw-Hill, New York.
[2] Van't Riet, K., and Smith, J. M., 1975, "The Trailing Vortex System Produced by Rushton Turbine Agitators," Chem. Eng. Sci., **30**, pp. 1093–1105.
[3] Yianneskis, M., and Whitelaw, J. H., 1993, "On the Structure of the Trailing Vortices Around Rushton Turbine Blades," Trans. Inst. Chem. Eng., Part A, **71**, pp. 534–550.
[4] Schafer, M., Yianneskis, M., Wachter, P., and Durst, F., 1998, "Trailing Vortices Around a 45° Pitched-Blade Impeller," AIChE J., **44**(6), pp. 1233–1246.
[5] Derksen, J. J., Doelman, M. S., and Van den Akker, H. E. A., 1999, "Three-Dimensional LDA Measurements in the Impeller Region of a Turbulently Stirred Tank," Exp. Fluids, **27**, pp. 522–532.
[6] Ranade, V. V., and Joshi, J. B., 1989, "Flow Generated by Pitched Blade Turbines I: Measurements Using Laser Doppler Anemometer," Chem. Eng. Commun., **81**, pp. 197–224.
[7] Mao, D.-M., Feng, L.-F., Wang, K., and Li, Y.-L., 1997, "The Mean Flow Field Generated by a Pitched Blade Turbine: Changes in the Circulation Pattern due to Impeller Geometry," Can. J. Chem. Eng., **75**, pp. 307–316.
[8] Jaworski, Z., Nienow, A. W., Koutsakos, E., Dyster, K., and Bujalski, W., 1991, "A LDA Study of Turbulent Flow in a Baffled Vessel Agitated by a Pitched Blade Turbine," Trans. Inst. Chem. Eng., Part A, **69**, pp. 313–320.
[9] Kresta, S. M., and Wood, P. E., 1993, "The Mean Flow Field Produced by a 45° Pitched Blade Turbine: Change in the Circulation Pattern due to Off Bottom Clearance," Can. J. Chem. Eng., **71**, pp. 42–53.
[10] Nouri, J. M., and Whitelaw, J. H., 1990, "Flow Characteristics of Stirred Reactors With Newtonian and Non-Newtonian Fluids," AIChE J., **36**(4), pp. 627–629.
[11] Hockey, R. M., and Nouri, J. M., 1996, "Turbulent Flow in a Baffled Vessel Stirred by a 60° Pitched Blade Impeller," Chem. Eng. Sci., **51**(19), pp. 4405–4421.
[12] Wechsler, K., Breuer, M., and Durst, F., 1999, "Steady and Unsteady Computations of Turbulent Flows Induced by a 4/45° Pitched-Blade Impeller," J. Fluids Eng., **121**, pp. 318–329.
[13] Ranade, V. V., Joshi, J. B., and Marathe, A. G., 1989, "Flow Generated by Pitched Blade Turbines II: Simulation Using k-ϵ Model," Chem. Eng. Commun., **81**, pp. 225–248.
[14] Ranade, V. V., Bourne, J. R., and Joshi, J. B., 1991, "Fluid Mechanics and Blending in Agitated Tanks," Chem. Eng. Sci., **46**(8), pp. 1883–1893.
[15] Bakker, A., Myers, K. J., Ward, R. W., and Lee, C. K., 1996, "The Laminar and Turbulent Flow Pattern of a Pitched Blade Turbine," Trans. Inst. Chem. Eng., Part A, **74**, pp. 485–491.
[16] Armenante, P. M., Luo, C., Chou, C.-C., Fort, I., and Medek, J., 1997, "Velocity Profiles in a Closed, Unbaffled Vessel: Comparison Between Experimental LDA Data and Numerical CFD Predictions," Chem. Eng. Sci., **52**(20), pp. 3483–3492.
[17] Sheng, J., Meng, H., and Fox, R. O., 1998, "Validation of CFD Simulations of a Stirred Tank Using Particle Velocimetry Data," Can. J. Chem. Eng., **76**, pp. 611–625.
[18] Xu, Y., and McGrath, G., 1996, "CFD Predictions of Stirred Tank, Flows," Trans. Inst. Chem. Eng., Part A, **74**, pp. 471–475.
[19] Ranade, V. V., and Dommeti, S. M. S., 1996, "Computational Snapshot of Flow Generated by Axial Impellers in Baffled Stirred Vessels," Trans. Inst. Chem. Eng., Part A, **74**, pp. 476–484.
[20] Harvey, A. D., Lee, C. K., and Rogers, S. E., 1995, "Steady-State Modeling and Experimental Measurement of a Baffled Impeller Stirred Tank," AIChE J., **41**(10), pp. 2177–2186.
[21] Jenne, M., and Reuss, M., 1999, "A Critical Assessment on the Use of k-ε Turbulence Models for Simulation of the Turbulent Liquid Flow Influenced by a Rushton-Turbine in Baffled Stirred-Tank Reactors," Chem. Eng. Sci., **54**, pp. 3921–3941.
[22] Jones, R. M., Harvey, III, A. D., and Acharya, S., 2001, "Two-Equation Turbulence Modeling for Impeller Stirred Tanks," J. Fluids Eng., **123**, pp. 640–648.
[23] Launder, B. E., and Spalding, D., 1974, "The Numerical Computation of Turbulent Flows," Comput. Methods Appl. Mech. Eng., **3**, pp. 269–289.
[24] Tsui, Y.-Y., and Pan, Y.-F., 2006, "A Pressure-Correction Method for Incompressible Flow Using Unstructured Meshes," Numer. Heat Transfer, Part B, **49**, pp. 43–65.
[25] Dong, L., Johansen, S. T., and Engh, T. A., 1994, "Flow Induced by an Impeller in an Unbaffled Tank-I. Experimental," Chem. Eng. Sci., **49**(4), pp. 549–560.